

Virtual skin: a behavioral approach helps verification

Dr. Benjamin NICOLLE, Arnaud LEGENDRE
Systems'Virtual Prototyping
300, route des Crêtes
Les Espaces Antipolis
F-06560 Sophia Antipolis
+33811036094

benjamin.nicolle@systemsvip.com

Dr. Louis FERRERO, Pr. Leonhard ZASTROW
Lancaster S.A.M.
Division of Coty
2, rue de la Lujernetta
MC-98000 MONACO
+37792050987

louis_ferrero@cotyinc.com

ABSTRACT

The aim of this study is to develop a new kind of R&D methodology through a VHDL-AMS functional virtual prototype (FVP) applied to cosmetic industries. Cosmetic firms are in the process of improving R&D methodologies with more formal methods. These studies are mostly based on functional models and less laboratory testing. Hence, in cooperation with Lancaster firm, we have built for the first time a unique dynamic model of biophysical and chemical phenomena linked to human skin and sun spectrum.

Human health can be strongly influenced by exposure to solar radiation. Relevant interactions regarding to health take place mainly in the skin. So, the optics of human skin is of the utmost importance with reflection and absorption properties. By combining a sun emission light model and a bio-optical human skin model, we can compute the effects of the sun radiations on various species including free radicals generation.

General Terms

Theory, Design, Verification, Performance.

Keywords

solar simulator, human skin, free radicals, reactive oxygen species, VHDL-AMS, functional virtual prototyping, multi-disciplines.

1. INTRODUCTION

Sunlight (especially UVA-Visible penetrating deeper into the skin [1]) has a profound effect on the skin causing skin ageing, skin cancer, and a host of skin changes. Many skin changes that were commonly believed to be due to ageing, such as easy bruising, are actually a result of prolonged exposure to sun radiation. Both UV and visible radiations can cause skin damage including wrinkles, lowered immunity against infection, ageing skin disorders and cancers. Some of the possible mechanisms for skin damage are collagen breakdown, formation of free radicals, interfering with DNA natural repairing flow rate, and inhibiting the immune system. This chain reaction (the lipid peroxydation) is initiated after a threshold time and is continued after the sun exposure. The understanding of the lipid peroxydation as a whole and often the interpretation of experimental results are made difficult by the complexity of the process. This complexity manifests itself both at the functional (behavior of the system) and at the structural level (the reactional network). The integration of different domains as thermics, biology, chemistry

etc increases the system complexity understanding. In such situations, a functional virtual prototype can synthesize the whole system and the multi-domains interactions. It can improve the understanding about overall properties of the skin system, helps the interpretation of experiments, and allow the estimation of magnitudes that are difficult to measure experimentally. The comparison of experimental results with model simulations can give hints about the limitations of current knowledge of the skin system under study and even suggests alternative interpretations and new experimental approaches as "the missing link - light-induced (280-1600 nm)" [2] which reveals the light spectrum as a major contributor (including UV).

The complete model is generic and written in VHDL-AMS, an IEEE-standardized Hardware Description Language (HDL) [3]. This language was developed to support the description and simulation of analog and mixed-signal circuits and systems from VHDL [4]. Such as MAST, Matlab, Modelica, it allows high level of abstraction and helps to reduce simulation times, but in addition facilitates the multi-level and multi-physics system description: it is a system oriented language, parameters and structures can be quickly and easily modified. This language allows to model discrete time behavior (as VHDL) and continuous time behavior with differential algebraic equations (DAEs) [5].

Therefore, we have divided the whole system in three main blocks as explained on figure 1 for complexity, domains management purpose: sun simulator, skin interactions, chromophores (sensitizers) and chemical reactions in the skin.

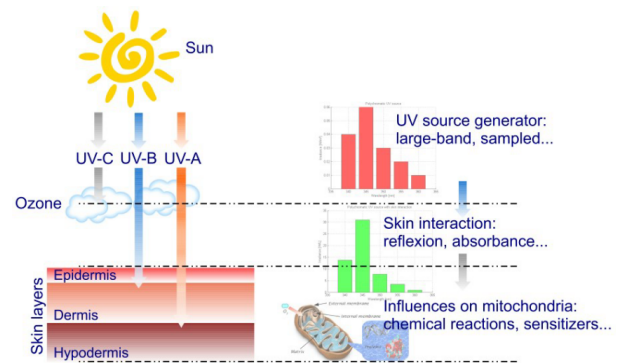


Figure 1: model and its environment architecture

The first part of this paper is focused on block modeling and its relative theory. The second part presents major simulation results compared to measurements.

2. HETEROGENEOUS SYSTEM ARCHITECTURE

2.1 Sun source simulator

To reflect the sun behavior experimentally, skin samples are exposed to radiation from artificial sources in UV and visible spectral bands with a sun simulator. The reference values of sun irradiance is defined with the ISO CIE 85 values. The sun gives off radiation that we divide into categories according to the wavelength:

- UVC (100 to 290 nm): UVC radiation is almost completely absorbed by the ozone layer and does not affect the skin.

- UVB (290 to 320 nm): UVB affects the outer layer of skin, the epidermis, and is the primary agent responsible for sunburns. Its intensity peak is between 10:00 am and 2:00 pm when the sunlight is the brightest. Its irradiance is also more intense in the summer months accounting for 70 % of a person's yearly UVB dose.

- UVA (320 to 400 nm): UVA was once thought to have a minor effect on skin damage, but now studies show that UVA is a major contributor to skin damage. UVA penetrates deeper into the skin and interacts efficiently with the skin cells. The intensity of UVA radiation is more stable than UVB without the variations during the day and throughout the year.

- Visible and IR (400 to > 750 nm): This spectrum is assumed, by the cosmetic and dermatologic community, to have a low impact over the skin sunburn. However the molar absorption coefficients of fewer chromophores reveals an important singlet oxygen flow rate generation in visible spectral part.

The interesting CIE spectral band is defined between 300 nm and 830 nm including UVA, UVB, visible and IRA parts. The sun generator model is a polychromatic model implementing different monochromatic sources with a pre-defined step value with generate function as defined on listing 1.

Listing 1. Use of generate instruction for polychromatic source

```

...
-- generate instantiation
gen_source : for I in 1 to N_source generate
  uv_src : entity WORK.mono_source(arch)
    generic map ( wiremesh => wiremesh,           -- wiremesh value
                  low_power => low_power,         -- low power level
                  high_power => power_uv(I),     -- high power level
                  time_delay => time_delay,       -- initial delay [s]
                  time_rise => time_rise,         -- rise time [s]
                  time_fall => time_fall,        -- fall time [s]
                  time_high => time_high,        -- time duration
                  time_period => time_period)    -- time period [s]
    port map ( q_intensity_uv => q_power_time(I)); -- UV source
  end generate;
end architecture str;

```

We can as well adjust the starting, ending, stepping values and the corresponding sun irradiances. Each monochromatic source can be refined with rise, fall times and multiple exposures (over a time period).

2.2 Skin interactions

The Skin PhotoType or SPT is a classification system based on a person's sensitivity to sunlight. People with skin types I and II are at the highest risk for photo-ageing effects including wrinkles and skin cancer. However, sun effects including wrinkles and skin cancer can occur in any skin type. This study is focused on a SPT IV skin characteristics but our model can be adapted to others SPT. The SPT IV characterizes a skin that burns minimally, always tans well to moderately brown.

2.2.1 Skin reflection

The skin reflection is linked to the source wavelength and the skin phototypes. We use a polynomial approach to model the reflection skin capabilities linked to the wavelength value (λ) with (1):

$$R_{skin} = C_2 \cdot \lambda^2 + C_1 \cdot \lambda + C_0 \quad (1)$$

where C_i coefficients are adapted for SPT IV. Therefore, the polychromatic transmitted ray is computed with the same wavelength step. We applied the equation (2) to sun irradiances:

$$I_{absorbed}(\lambda) = I_{fromsun}(\lambda) * (1 - R_{skin}(\lambda)) \quad (2)$$

2.2.2 Skin transmittance

The skin does not present the same thickness and the same exposure to sun. For example, the dorsal side of the forearm is a skin area that is naturally exposed to sunlight in the summer months. Related to irradiance wavelength value, the skin have a transmittance linked to its depth. We try to define the different transmittance laws linked the spectrum. Based on literature [6], we use (3) equation and different a, b coefficients to obtain figure 2.

$$T_{skin}(d_{skin}, \lambda) = 1 - (a(\lambda) * e^{-\frac{b(\lambda)}{d_{skin}}}) \quad (3)$$

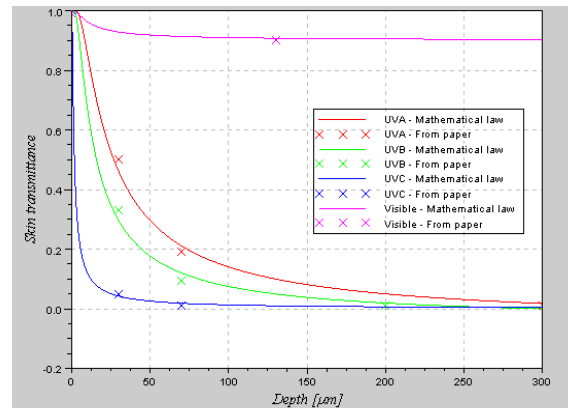


Figure 2: skin transmittance for different spectrum band

We have to implement smoothing functions to map the reality. Therefore, we use segmented-functions based on spectral domains. Different equations are implemented using previous a, b coefficients. By plotting the transmittance model with this smooth approach, figure 3 will focus on UVA, UVB and visible spectral parts for a SPT IV skin. We use this model during the next studies.

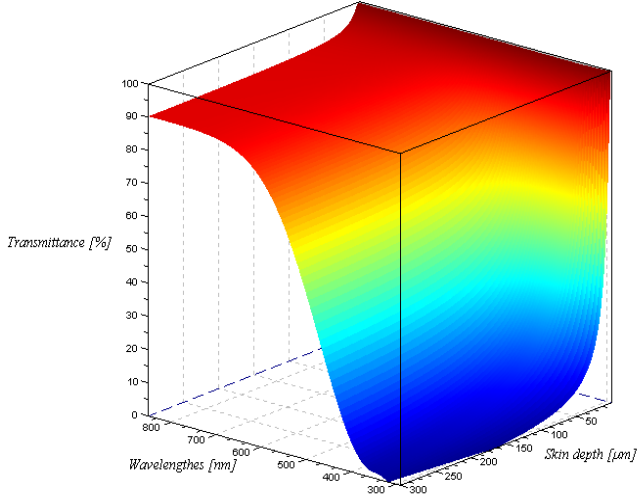


Figure 3: skin transmittance model with smoothing functions

2.2.3 Surface to Volume conversion

In fact, the skin is a volume and not a surface. Hence, instead of irradiance notion expressed in W/m^2 , the rate concentration introduced in sensitizers is M/L . In a first step, we propose to link surface and volume. We need to compute on each wavelength the corresponding volume irradiance linked to d_{skin} with surface irradiance integration over the skin depth (4):

$$I_{\left[\frac{W}{m^2}\right]} = \int_0^{d_{skin}} I_{\left[\frac{W}{m^2}\right]}(d_{skin}) dd_{skin} \quad (4)$$

The surface irradiance is defined with (5):

$$I_{\left[\frac{W}{m^2}\right]} = I_{\left[\frac{W}{m^2}\right]}(0) \cdot T_{skin}(d_{skin}, \lambda) \quad (5)$$

Since $1000 L = 1 m^3$, to compute the absorbed power in W/L at the skin observation point (for example, dermis and epidermis limit - $130 \mu m$), the surface to volume conversion is used according to figure 3 and equation (6):

$$I_{absorbed\left[\frac{W}{L}\right]} = 10^{-3} \cdot I_{sun\left[\frac{W}{m^2}\right]}(0) * \int_0^{d_{skin}} (1 - (a(\lambda) \cdot \exp\left(\frac{-b(\lambda)}{d_{skin}}\right))) dd_{skin} \quad (6)$$

The integration result is given by (7):

$$\begin{aligned} & \int (1 - (a(\lambda) \cdot \exp\left(\frac{-b(\lambda)}{d_{skin}}\right))) dd_{skin} \\ &= -a \exp\left(\frac{-b}{d_{skin}}\right) \cdot d_{skin} + d_{skin} - a \cdot b \cdot Ei\left(\frac{-b}{d_{skin}}\right) \end{aligned} \quad (7)$$

where Ei is the exponential integral. The result of this integration is a complex result. Then, another solution to compute this integral consists in introducing a sum function which computes the transmittance integration, driving to a relatively small computing error given by (8):

$$\begin{aligned} & \int (1 - (a(\lambda) \cdot \exp\left(\frac{-b(\lambda)}{d_{skin}}\right))) dd_{skin} \\ &= \sum_{x=0\mu m}^{d_{skin}} T(\lambda, x) \cdot x \end{aligned} \quad (8)$$

In this case, we obtain an error for $d_{skin} = 130 \mu m$ and $1 \mu m$ step value about 1.2 % for UVA, 2 % for UVB and 0.8 % for visible between the numeric integral computation (using a function based on loop instruction - listing 2) and this approach. Therefore, the final equation for surface to volume conversion is (9):

$$I_{absorbed\left[\frac{W}{L}\right]} = 10^{-3} \cdot I_{fromsun\left[\frac{W}{m^2}\right]}(0) * \sum_{n=0}^{d_{skin}/step} T(\lambda, n \cdot step) \cdot (n \cdot step) \quad (9)$$

Listing 2. Surface to Volume conversion using function & loop instructions
function transmittance_integration (skmin, skstep : real; instep : integer)

```

return real is
  variable term, t_int, skin_step : real := 0.0;
begin
  int_loop : for step_int in 0 to index_max loop
    -- compute the skin depth value
    skin_step := skmin + skstep * real(instep);
    -- compute the transmittance
    term := 1.0 - (a_factor * exp(b_factor/(-skin_step)));
    -- compute the sum
    t_int := t_int + term * skstep; -- integral = integral_before + T*step
  end loop;
  return t_int;
end function transmittance_integration;

```

2.3 Skin photosensitizer

The first law of photochemistry states that “only light absorbed by a molecule can produce photochemical change in that molecule”. When light encounters a molecule, it can either be scattered or absorbed. A molecule (S) that has absorbed a quantum of light is said to be excited and molecules that can be excited by absorption of visible light are named chromophores or photosensitizers (S*). The absorption spectrum of a molecule reflects its probability of transition between the ground state and any of the vibrational and rotational levels of its first and higher excited states. The absorption spectrum, characterized by the molar absorption coefficient ϵ_s at a particular wavelength, is described by Beer-Lambert's law (10):

$$A(\lambda) = -\log_{10}\left(\frac{I_{transmitted}(\lambda)}{I_{incident}(\lambda)}\right) = \epsilon_s(\lambda) * d_{skin} * [S]_{initial} \quad (10)$$

Photochemistry occurs when an excited sensitizer S* interacts with other molecules. Most commonly, these molecules are oxygen, O_2 . The excited sensitizer S* may transfer either energy or charge during interactions with this kind of molecules. The various possibilities are shown in the figure 4 below.

The mechanisms responsible for photosensitized oxydations have been classified into two categories, called Type I and Type II reactions. This is general agreement that reactions generating free-radicals from a target molecule should be classified as Type I photochemistry. Similarly, singlet-oxygen (1O_2) generation should be classified as Type II photochemistry. We focused here on type II effect. Riboflavin plays a significant role in the oxydation process as a photosensitizer [7].

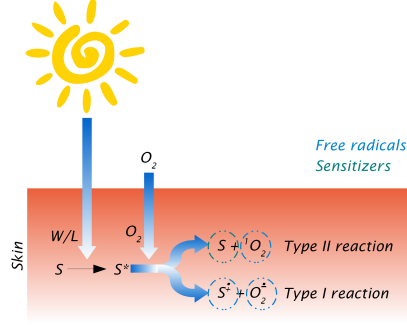


Figure 4: oxygen and radicals generation

According to this paper and based on the previous theory, one sensitizer, as riboflavin, has been characterized. The riboflavin chromophore has a polychromatic molar absorption [8]. According to Beer-Lambert's law, the transmission factor is expressed in terms of an absorbance A which for liquids is defined as (11):

$$A(\lambda) = -\log_{10}\left(\frac{I_{\text{absorbed}}(\lambda)}{I_{\text{incident}}(\lambda)}\right) \quad (11)$$

This implies that the absorbance becomes linear with the concentration (or number density of absorbers, here riboflavin) at wavelength value λ according to (12):

$$A(\lambda) = \epsilon_{\text{Riboflavin}}(\lambda) * d_{\text{skin}} * [RF]_{\text{initial}} \quad (12)$$

So, the excited riboflavin concentration is (13):

$$[RF]_{\text{excited}} = \Phi_T * I(d_{\text{skin}}, \lambda) * A(\lambda) \quad (13)$$

2.4 Chemical equations

We focus our study on the mitochondria cell as it is one of the best-described biological entity in the literature. Moreover, integrative models on this cell have already been realized by [9], and most of the reaction rate constants and species concentrations are available. Mitochondria cells (figure 5 presents a cross section) are founded in a high concentration in the derm and many works have tried to link the skin aging to a dysfunctional of the dermal mitochondria [10].

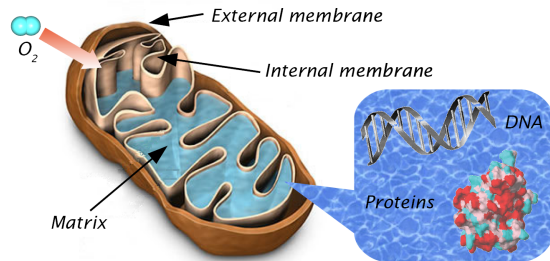


Figure 5: mitochondria cross section

When the excited sensitizer interacts with an oxygen, it creates a reactive oxygen species (ROS) which can initiate a lipid chain reaction upon sun radiance. Human skin defenses are included in the model as E vitamin, glutathione, etc. We implemented as a first step, 96 chemical reactions using a 1st order approximation. We use a species dictionary and a code generator based on chemical equations. Therefore, this model can evolve easily to

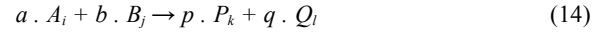
introduce more reactions. Next step is to implement 10K chemical equations to increase skin model accuracy.

The model considers an aqueous and a membrane compartment. We assume that most species are present in only one of the phase as described on table 1. The exception are O_2 , protein and perhydroxyl radical (HO_2).

Table 1. Species compartmentation

Aqueous phase	Membrane phase
$O_2\text{aq}$, $HO\cdot$, $O_2\cdot^-$, $HO_2\cdot$, H_2O_2 , Fe^{2+} , Fe^{3+} , $SOD-Mn^{3+}$, $SOD-Mn^{2+}$, $CatFe^{2+}$ $AscH\cdot$, $Asc\cdot^-$, Asc , GSH , $GSSG$, $GPXrd$, $GPXo$, $GSGPX$, $PHGPXrd$, $PHGPXo$, $GSPHGPX$ protein, DNA	O_2m , $HO_2\cdot$, $P-LH$, $P-L\cdot$, $P-LOO\cdot$, $P-LO\cdot$, $P-LOOH$, $PLOH$, $LOOH$, LOH $TocOH$, $TocO\cdot$, $UbqH_2$ protein

Concerning the pH, a constant value of 6 was considered as a compromise between a pH around 5 near the membranes and a neutral environment in the bulk aqueous phase. Oxygen is also considered to be present in both lipid and aqueous compartments. The model assumes a concentration of 35 μM at the aqueous phase. For the lipid phase, literature [9] gives a 105 μM concentration. Some reactions of the model involve species from different compartments. The calculation of the rates of production or consumption due to these reactions must take into account the volumes of each compartment. If we consider an interface reaction involving species in different compartments (the subscripts stand for the compartment where each species is located) (14):



The relationships (15):

$$\frac{1}{a} \frac{dn_A}{dt} = \frac{1}{b} \frac{dn_B}{dt} = -\frac{1}{p} \frac{dn_P}{dt} = -\frac{1}{q} \frac{dn_Q}{dt} \quad (15)$$

where n_X stands for the quantity of species X, always held, independently from the distribution of the species by the compartments. Therefore, the changes in the concentrations, are related as (16):

$$\frac{V_i}{a} \frac{d[A]_i}{dt} = \frac{V_j}{b} \frac{d[B]_j}{dt} = -\frac{V_k}{p} \frac{d[P]_k}{dt} = -\frac{V_l}{q} \frac{d[Q]_l}{dt} \quad (16)$$

where V_x stands for the volume of compartment X.

Consider now that i and k refer to the membrane phase and j and l to the aqueous phase (17):

$$-\frac{1}{a} \frac{d[A]_m}{dt} = k \Gamma_m^{(a-1)} \Gamma_{aq}^b [A]_m^a [B]_{aq}^b \quad (17)$$

with

$$\Gamma_m = \frac{V_m}{(V_m + V_{aq})} \quad \Gamma_{aq} = \frac{V_{aq}}{(V_m + V_{aq})}$$

This ratio was applied to the model.

3. SIMULATION RESULTS

3.1 Irradiance evolutions

We focus our simulation results on the sun CIE norm. Based on CIE wavelength and irradiance values, the sun generator has been simulated on figure 6.

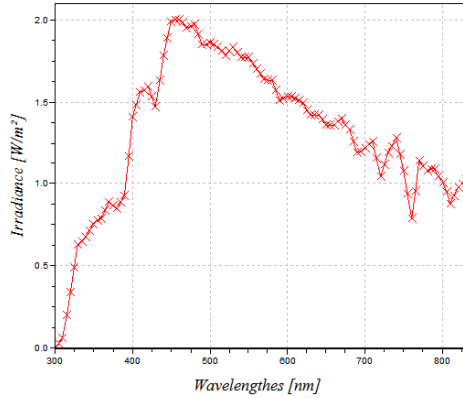


Figure 6: sun CIE irradiances versus wavelengths

The absorbed (after reflection) irradiances are computed with the polynomial approach. These irradiances are surface irradiances in W/m^2 . We apply these absorbed irradiances with polychromatic capability at different skin depth levels between 0 and 300 μm (surface to volume conversion). The volume irradiances are expressed in W/L . For each skin depth level d_{skin} and surface irradiance, we compute the transmittance integration between 0 μm and d_{skin} linked to a volume based on these parameters. We obtain the results given by figure 7.

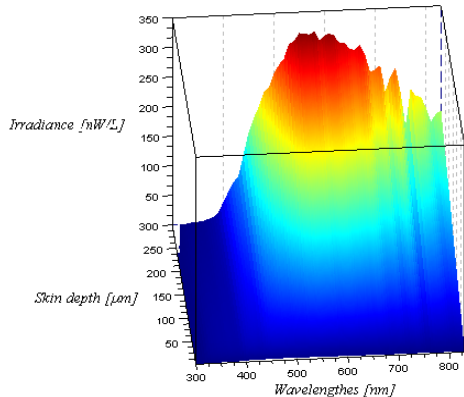


Figure 7: Transmitted irradiances in CIE case

The irradiance plotted on this figure are volume irradiance in W/L : it increases with the skin depth level due to a transmittance integration rise. The shape reveals :

- peak values between 500 and 600 nm (visible spectrum part),
- quick increases for skin depth level higher than 150 μm ,
- spectral jamming for UVA and visible.

3.2 Singlet oxygen flow rate simulations

The riboflavin contribution will be simulated with sun CIE volume irradiances. This part is focused on riboflavin initial concentration parameter adjustment. Based on total mitochondria O_2 concentration, 140 $\mu M/L$ from [9], we simulated the influence of the CIE volume irradiances on a polychromatic riboflavin chromophore at different skin depth levels (between 0 and 300

μm). As described on figure 8, the parameters choice induces a 6x factor between the peak values in the two cases. The singlet oxygen generation linked to riboflavin chromophore is concentrated in the 400-500 nm spectrum part for the two cases. Hence, the visible spectrum is an important contributor to singlet oxygen generation and therefore, lipid peroxydation with this chromophore. We choose the higher values couple for the next studies including riboflavin chromophore due to an important generation for dermis-epidermis limit ($\sim 130 \mu m$) in UVA - visible spectrum.

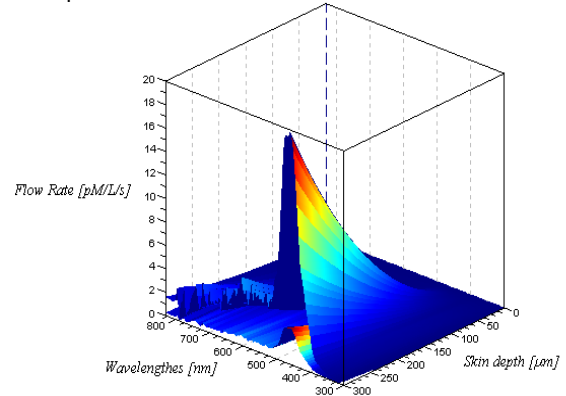


Figure 8: Riboflavin singlet oxygen flow rate generation

3.3 Steady State system response

The first expected result is the steady state (SST) of our system. The aim of this simulation is to determine the different rate concentrations in a steady state case matched to skin typical values. Full results will be showed in the presentation.

3.4 Lipid peroxydation initiation

In this part, we want to validate a lipid peroxydation with the species concentrations extracted from previous SST. Using previous initial riboflavin concentration, we simulate the time species evolution with the CIE spectrum values on figure 9.

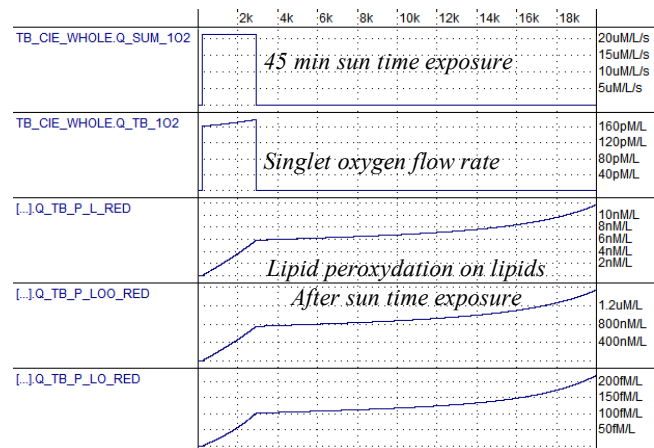


Figure 9: Lipid peroxydation initiation

This initial rate concentration is not well documented in the literature. We simulate a sun exposition with CIE contribution around 45 min to obtain the lipid peroxydation (and sunburn) which corresponds to Lancaster knowledge (species concentration in Mol/Liter). In these conditions, the initial species concentrations are the main triggers on the lipid

peroxydation initiation. As we demonstrated in [11], iron, riboflavin and human defenses concentration are the major contributors.

3.5 Time threshold and free radicals

The purpose of this study is to determine the time threshold capability which initiates the chain reaction on the free radicals particularly on the lipids. Based on a classical time simulation, we change the sun time exposure from 500 to 10000 seconds with a 500 s step. Then, we measure the lipid radical species concentration at the end of the sun time exposure and 1000 seconds after the sun time exposure. Therefore, we compute the acceleration ratio percentage which characterizes the chain reaction initiation. We compute the fatty acyl carbon centred radical (L_red), esterified fatty alcoxyl radical (LO_red), esterified fatty acyl peroxy radical (LOO_red) concentration at the end of the sun exposure and 1000 seconds after it. We compute the percentage between these two values which characterizes the lipid peroxydation initiation when the factor is positive. These three factors (for each radical species) are plotted on figure 10.

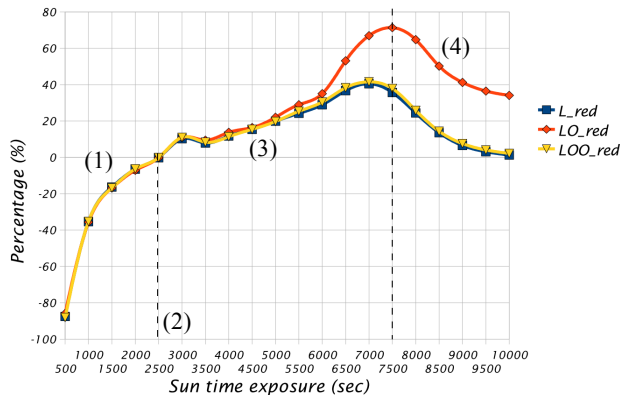


Figure 10: acceleration ratio 1ks after sun exposure

We observe four different areas on this figure:

- (1): in the first area, the lipid peroxydation does not initiate due to sun time exposure less than the time threshold value,
- (2): the 2700 seconds time threshold initiates the lipid peroxydation and the chain reaction will increase slowly the free radicals concentration values,
- (3): the chain reaction increases significantly the LO_red radical concentration (with a maximal peak +70%/7500 seconds). L_red and LOO_red present the same behavior linked to the chain reaction and the same chain reaction peak +40% for 7000 seconds.
- (4): after these peak behaviors and 7500 seconds sun time exposure threshold, the chain reaction phenomena will decrease.

4. CONCLUSION

This study presents the capability to map a complex functional skin model and its environment to simulate it dynamically taking a part of the sunlight spectrum based on a standard sun (CIE) or based on a Lancaster sun simulator (ORIEL) as the chain reaction initiator.

For this purpose, we have divided the whole system in three blocks for complexity management: sun spectrum, skin

interaction, chromophores and chemical reactions in the skin. The skin phototype and absorption have been implemented, focused here on a SPT IV skin. We get a maximal error about 2% for the absorption computation (with the surface to volume conversion). Finally, the mitochondria cell have been modeled. We have demonstrated the visible contribution of the riboflavin chromophore on the lipid peroxydation initiation.

The discussion on why AMS simulator as Smash and behavioral language as VHDL-AMS will be addressed during the conference presentation.

5. ACKNOWLEDGMENTS

This work have been done with Smash software and on demand and with Lancaster-Coty experts. We want to thank Dolphin Integration for their support.

6. REFERENCES

- [1] L. Zastrow et al. - "Detection and identification of Free radicals generated by UV and Visible Light in Ex Vivo Human Skin" - IFSCC Magazine - Vol.11, n°3/2008 - pp. 207-215
- [2] L. Zastrow et al. - "The Missing Link - Light-Induced (280-1600 nm) Free Radical Formation in Human Skin" - Skin Pharmacol Physiol - Vol. 22 - pp. 31-44
- [3] IEEE Computer Society "IEEE Standard VHDL Analog and Mixed-Signal Extensions". Design Automation Standards Committee of the IEEE Computer, Society. IEEE Std 1076.1-1999
- [4] Peter J. Ashenden et al. - "The system designer's guide to VHDL-AMS" - Morgan Kaufman Publishers, 2003
- [5] F. Pêcheux et al., "VHDL-AMS and Verilog-AMS as Alternative Hardware Description Languages for Efficient Modeling of Multidiscipline System", IEEE TCAD, vol. 24, No. 2, Feb. 2005
- [6] Kristian P. Nielsen et al. - "The optics of human skin: aspects important for human health" - Solar Radiation and Human Health, Espen Bjertness editor, The Norwegian Academy of Science and Letters, 2008, pp. 35-46
- [7] DeMan "Principles of Food Chemistry", 3rd Ed., Aspen Publishing Company, 1999, Gaithersburg
- [8] Jurgen Baier et al., "Singlet Oxygen Generation by UVA Light Exposure of Endogenous Photosensitizers", Biophysical Journal - August 2006 - pp. 1452-1459
- [9] F. Antunes et al., "Lipid peroxydation in mitochondrial inner membranes. I. An integrative kinetic model", Free radical biology & medicine, 1996, Vol. 21, No. 7, pp. 917-943
- [10] Berneburg et al., "Singlet Oxygen Mediates the UVA-induced Generation of the Photoaging-associated Mitochondrial Common Deletion", The journal of biological chemistry, Vol. 274, No. 22, May 1999, pp. 15345-15349
- [11] B. Nicolle et al., "From UVA to the Lipid Chain Reaction : Archetype of a Virtual Skin Model" - HSC'08 - October 22, 2008.